Geophysical Research Letters

RESEARCH LETTER
10.1029/2023GL104123

# On the Relation Between Jupiter's Aurora and the Dawnside Current Sheet

**Y. Xu[1,2,3], Z. H. Yao[1,2,4], B. Zhang[5], P. A. Delamere[6], L. C. Ray[3], W. R. Dunn[4], S. V. Badman[3], E. H. Feng[5], Z. Q. Zheng[5], S. J. Bolton[7], D. Grodent[8], B. Bonfond[8], and Y. Wei[1,2]**

[1]Key Laboratory of Earth and Planetary Physics, Institute of Geology and Geophysics, Chinese Academy of Sciences, Beijing, China, [2]College of Earth and Planetary Sciences, University of Chinese Academy of Sciences, Beijing, China, [3]Department of Physics, Lancaster University, Lancaster, UK, [4]Department of Physics and Astronomy, University College London, London, UK, [5]Department of Earth Sciences, University of Hong Kong, Pokfulam, China, [6]Department of Physics, University of Alaska Fairbanks, Fairbanks, AK, USA, [7]Southwest Research Institute, San Antonio, TX, USA, [8]Laboratoire de Physique Atmosphérique et Planétaire, STAR Institute, Université de Liège, Liège, Belgium

**Key Points:**

- The features of the current sheet in Jupiter's dawnside magnetosphere are highly relevant to auroral contexts
- During a solar wind compression event, the dawnside current sheet becomes substantially thinner than during quiet times
- The total current intensity of the current sheet is much higher during solar wind compression events than the quiet times

**Supporting Information:**

Supporting Information may be found in the online version of this article.

**Correspondence to:**

Z. H. Yao,
z.yao@ucl.ac.uk

**Citation:**

Xu, Y., Yao, Z. H., Zhang, B., Delamere, P. A., Ray, L. C., Dunn, W. R., et al. (2023). On the relation between Jupiter's aurora and the dawnside current sheet. *Geophysical Research Letters*, *50*, e2023GL104123. https://doi.org/10.1029/2023GL104123

Received 13 APR 2023
Accepted 26 JUN 2023

**Abstract** Jupiter's auroral emission is a spectacular phenomenon that provides insight into energy release processes related to the coupling of its magnetosphere and ionosphere. This energy release is influenced by solar wind conditions. Using joint observations from Juno and the Hubble Space Telescope (HST), we statistically investigate the relationship between auroral power and current sheet variations under different solar wind conditions. In this study, we reveal that during global main auroral brightening events that are closely connected to solar wind compressions, the dawn side current sheet is substantially thinner than during times when a quiet auroral morphology is present. Furthermore, the total current intensity in the current sheet is found to increase under solar wind compression conditions compared to the quiet period. These findings provide important observational evidence for how magnetospheric dynamics driven by solar wind behavior affect auroral activity, deepening our understanding of the coupling between Jupiter's magnetosphere and ionosphere.

**Plain Language Summary** Jupiter, the largest planet in our solar system, has a fascinating and powerful auroral emission that can help us understand the interactions between its magnetic field and the charged particles in its atmosphere. These auroral emissions are influenced by solar wind conditions, which are streams of charged particles coming from the Sun. In this study, we used observations from the Juno spacecraft and the Hubble Space Telescope to investigate the relationship between Jupiter's auroral emissions and changes in the planet's magnetic field. We found that during periods of increased solar wind pressure, the magnetic field layer, known as the current sheet, becomes thinner compared to times when the aurora is quiet. These findings offer valuable evidence of how Jupiter's magnetic field is affected by solar wind behavior and improve our understanding of the relationship between the planet's magnetic field and its aurora. This research helps us better comprehend the complex processes occurring in Jupiter's magnetosphere and can potentially enhance our knowledge of similar phenomena occurring on other planets.

## 1. Introduction

Jupiter has the most intense magnetic field and powerful auroral emission in our solar system. Similar to the terrestrial magnetosphere, Jupiter's magnetosphere is formed by the interaction of the solar wind with the planet's global magnetic field. However, unlike the terrestrial system, Jupiter's magnetosphere is substantially inflated by internal plasma, primarily generated by the ionization of neutrals from the moon Io (e.g., Joy et al., 2002; Thomas et al., 2004). Jupiter's rapid rotation, combined with the plasma ejected into the magnetosphere by Io's volcanism, internally drives the Jovian system and produce a disclike plasma distribution, known as the plasmadisc (Connerney et al., 1981, 2020; Khurana & Schwarzl, 2005; Krupp et al., 2005; Mauk et al., 2004; Thomas et al., 2004). Over the past two decades, the Jovian main auroral emission has been attributed to the centrifugally-driven outflow of Io-genic plasma and its interaction with Jupiter through a large-scale magnetosphere-ionosphere (M-I) coupling current system (e.g., Badman et al., 2016; Cowley & Bunce, 2001; Cowley et al., 2007, 2017; Nichols & Cowley, 2003; Pensionerov, Cowley, et al., 2021; Ray et al., 2010, 2014; Southwood & Kivelson, 2001). The main auroral oval on Jupiter is intrinsically linked to the transfer of angular momentum from the planet to its magnetosphere (e.g., Hill, 1979). This transfer is facilitated by a centrifugally driven interchange instability that drives

plasma outward from Jupiter (Krupp et al., 2004), requiring the transfer of angular momentum from the planet to maintain the magnetospheric plasma velocity near corotation. Upward field-aligned currents (FACs) flow from Jupiter's ionosphere to the magnetosphere where they feed radially outward currents that play a crucial role in mediating the transfer of angular momentum. These generate an associated magnetospheric $\mathbf{j} \times \mathbf{B}$ force that accelerates the plasma toward corotation. Hence the M-I coupling and magnetodisc current systems are inextricably coupled. Statistical evidence of a strong correlation between Jupiter's northern dawnside main auroral emission and this magnetospheric equatorial radial current has been found through analysis of Juno magnetometer data and Hubble Space Telescope (HST) observations (Nichols & Cowley, 2022). Additionally, recent progress showed that Alfvénic wave power could also be an important source in driving Jupiter's aurora (e.g., Bonfond et al., 2020; Pan et al., 2021; Saur et al., 2018).

The characteristics of the main auroral emission under solar wind compression have been the subject of vigorous debate within the community. The anti-correlation of the intensity of the main oval with the solar wind dynamic pressure was first proposed by Cowley and Bunce (2001) and Southwood and Kivelson (2001). However, subsequent studies reported that the intensity of Jupiter's auroral emission enhances when the solar wind compresses the magnetosphere (e.g., Baron et al., 1996; Connerney et al., 1996; Gurnett et al., 2002; Nichols et al., 2017; Pryor et al., 2005; Sinclair et al., 2019; Yao et al., 2019, 2022), contrary to expectations. Grodent et al. (2018) classified the ultraviolet auroras observed by the HST into six main families based on auroral morphology. Two of these are the Q (Quiet) family thought to correspond to the calm magnetospheric state, and X (eXternal perturbation) family corresponding to an external perturbation to the magnetopause (e.g., a solar wind compression). This provides an essential basis for studying the relationship between the magnetospheric state and the aurora under solar wind compression. Yao et al. (2022) systematically utilized observations of Juno and the HST to build the relationship between auroral morphologies and compression conditions of Jupiter's magnetopause. They pointed out that main auroral brightening occurs in systematic ways under compressed magnetopause conditions, which corresponds to the "X" family of auroral events of Grodent et al. (2018). However, a comprehensive insight into the state of the magnetospheric current sheet when the aurora brightens under solar wind compression is still far from well understood, due to the lack of simultaneous observations of the aurora and the magnetosphere.

In this study, we perform a comprehensive investigation of dawnside current sheet crossing events by the Juno spacecraft with simultaneous auroral observations from the HST that may inform us on solar wind conditions following the suggestion in Grodent et al. (2018). And for the first time, we reveal statistical evidence of an increase in current intensity and thinning of the dawn-side current sheet under magnetospheric compressions. We note that although the terms "sheet" and "disc" are often interconnected in Jovian magnetosphere, this study mainly includes the calculation of the current intensity of an equatorial structure at a fixed local time across a large radial distance. As a result, we will utilize the term "sheet" instead of "disc" in this study.

## 2. Observations

The magnetic field in the Jovian magnetosphere is obtained from Juno's Magnetic Field investigation (MAG) (Connerney et al., 2017). Distributions of ions and electrons with energy >30 keV are measured in situ with Juno's Jupiter Energetic-Particle Detector Instrument (JEDI) (Mauk et al., 2017).

Using Table 1 of Grodent et al. (2018), 30 current sheet crossing events corresponding to 8 "Q" family auroras and 7 "X" family are selected for a comparative investigation. Each auroral observation time has been corrected for the light travel from the HST to Juno. Since the HST visits were not planned at the exact time when Juno crossed the current sheet, we sample two current sheet crossings for each auroral observation, that is, the one before the auroral observations and the one after. The two current sheet crossings are the most relevant magnetospheric observations associated with each HST visit. The physical connection between the observations of the current sheet crossings and auroral context is reasonable, because the bulk morphology of Jupiter's UV aurora is known to change over timescales ranging from tens of minutes to hours or more (Ballester et al., 1996; Gerard et al., 1994; Kimura et al., 2015, 2017; Kita et al., 2016; Yao et al., 2019, 2020). The tilt angle of Jupiter's magnetic axis relative to its rotation axis results in a periodic swinging of the current sheet for a fixed magnetospheric location. Therefore, the spacecraft near the magnetic equator would cross the current sheet twice in a rotation period (~10 hr). Hence, the spacecraft must cross the current sheet within 5 hr before or after each observation (see Figure 1). We take two crossings, before and after the HST observations, to be representative of the current sheet state during the auroral enhancement. We note that for auroral family X, the disturbed behavior and dusk

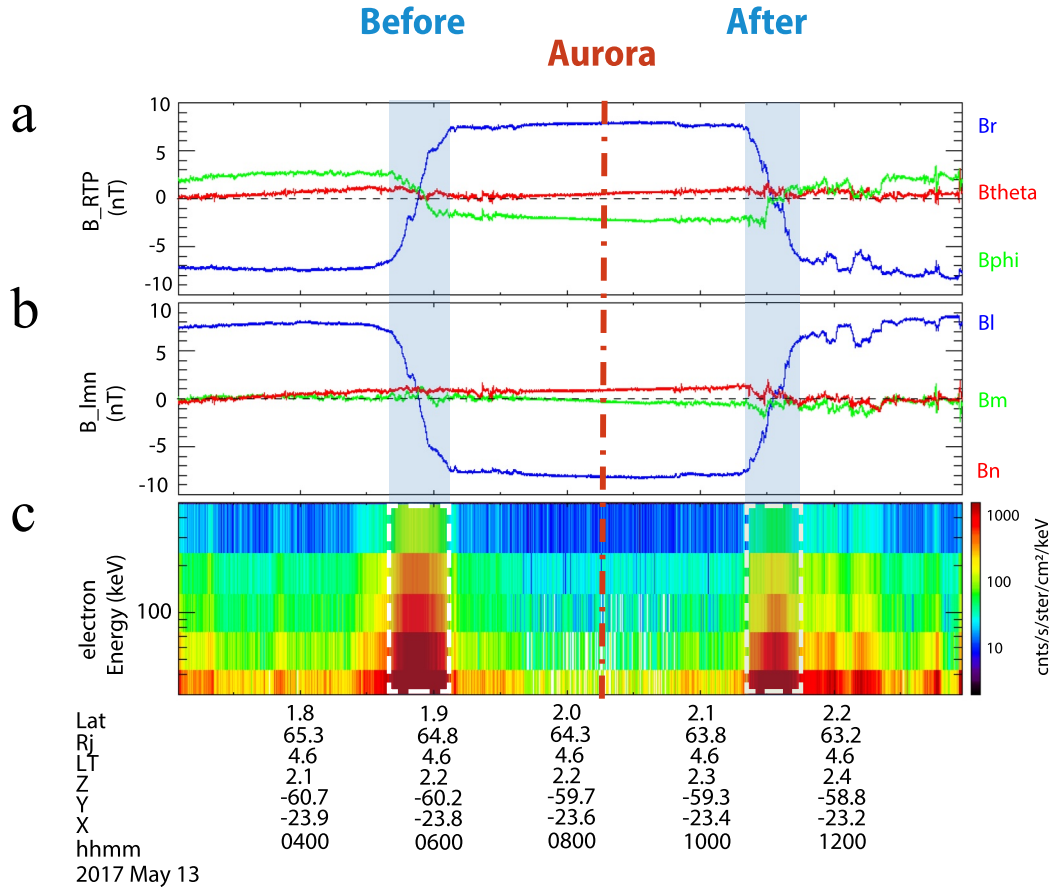


**Figure 1.** A current sheet crossing event during "quiet" aurora between 2:10 and 13:50 UT on 13 May 2017. (a) R-Theta-Phi magnetic field components in Jupiter-De-Spun-Sun (JSS) coordinate. (b) LMN magnetic field components in the field–aligned coordinates, obtained by performing minimum variance analysis. Panel (c) displays the energy spectrums of electrons. The location information at the bottom of the figure is in the JSS coordinate system. The blue shadings represent the current sheet crossing regions. The red dotted line is the corrected Juno time when the aurora was observed (see Table 1 of Grodent et al., 2018). The white dashed box marks the significantly enhanced electron energy spectrum during the current sheet crossing, which is used to determine current sheet crossing durations.

arcs of the aurora are observed to last longer than the ~5-hr window spanning the current sheet crossings (e.g., Dunn et al., 2020; Nichols et al., 2009, 2017; Yao et al., 2022). The duration of each crossing is used as a proxy for the current sheet thickness. Note that the relative speed of the current sheet flapping to the spacecraft could affect the proxy, and that this uncertainty cannot be eliminated with only a single spacecraft. And although the Khurana models (Khurana & Schwarzl, 2005) and the Pensionerov models (Pensionerov, Belenkaya, et al., 2021) allow the bending of the magnetodisc at a large radial distance toward the Jovigraphic equator, notably the results in this study are insensitive to such complications because we only compare the current sheet state at a set radial distance (50–80 $R_J$) between the quiet conditions and external perturbation conditions.

The magnitude of the magnetic field outside of the current sheet (i.e., $B_{lobe}$), can be used to infer the current intensity within the sheet. The radial distance of the crossing, $R$, was recorded to compare the positions of all events. All crossings were located in the dawn side, near 5 LT (5 ± 0.5) and at low latitudes (<5°, JSS coordinate system). The HST program GO-14634 provided an unprecedented opportunity to study the relationship between current sheet characteristics and the auroral context. Figure S1 in Supporting Information S1 shows the comparison of auroral observations under quiet and external perturbation conditions. In this study, the start and end points of the current sheet crossing are identified by manually selecting notable changes in the slope of the $B_l$ component, shown in Figure 1 as the blue-shaded regions. The enhancement of the electron energy spectrum is also considered as a crucial constraint in the identification process (see white-boxed regions in Figure 1c), particularly under external disturbance conditions. This is because under disturbance conditions, magnetic field signature associated

with the crossing can become ambiguous due to current sheet perturbations. In such cases, the enhancement or weakening of the electron energy spectrum provides a more precise and robust identification of the current sheet crossing region. The observations of all 30 current sheet crossings are provided in Supporting Information S1, and the crossing area for each event has been clearly identified (as shown in Figures S3–S17 in Supporting Information S1). Nonetheless, it should be noted that for some highly dynamic events under external perturbation conditions, the $B_l$ component and the electron energy spectrum may undergo drastic changes, making it challenging to determine the crossing duration precisely. To err on the side of caution, we use the combination of magnetic field and electron energy spectrum data to identify the start and end points of the current sheet crossing, by determining where the spacecraft first steadily exits and last steadily enters the lobe region, as shown in Figures S11, S15, and S17 in Supporting Information S1. $B_{\text{lobe}}$ is sampled before each current sheet crossing. Among all events, case 2 under external disturbance conditions is an extreme case, as shown in Figure S12 in Supporting Information S1. In this event, the spacecraft's position swaps between the current sheet and the lobe region before crossing, making it hard to sample $B_{\text{lobe}}$ accurately. In this case, we identify the divided lobe region and average the magnetic fields of these parts (as shown in Figure S12 in Supporting Information S1).

Figures 2 and 3 show the statistical distributions of current sheet crossing duration under different auroral morphologies that were believed to correspond to compressed and quiet magnetospheric conditions. Figure 2a shows the current sheet crossing duration and the magnetic field in the lobe region $B_{\text{lobe}}$ at different radial distances corresponding to aurora under quiet conditions, and Figure 2b displays events occurring during external perturbation. The $y$-axis represents $B_{\text{lobe}}$ before the crossing, and each circle's color and size represent the duration of the spacecraft crossing within the current sheet. In this study, the events were all near a fixed local time (~5 LT), and at low latitudes (<5°). At a given radial distance, it can be generally suggested that the shorter the duration, the thinner the current sheet. The magnitude of $B_{\text{lobe}}$ decreases toward larger distances, at a decreasing rate. The duration distribution of the current sheet crossings under quiet conditions shows a roughly inverse correlation trend before range of 65–70 $R_J$ (see colors and size of data points vs. radial distance in Figure 2). This aligns with the observations reported by Liu et al. (2021), which indicated that the half-thickness of the current sheet reaches a minimum around 65 $R_J$. In Figures 2a and 2b, we apply a description of the magnetic field magnitude as a function of radial distance in the form of $Ax^{-1} + Bx^{-5}$ (see the gray and blue dashed line) assuming the superposition of an ideally simplified Jupiter dipole field and a simple current sheet model. According to Ampère's circuital law the magnetic strength, $B$, produced by an infinitely large thin plane current in a single direction is related to the density of the line current, I, with the magnetic field direction parallel to the plane but perpendicular to the current direction

$$B = \mu_0 I/2 \tag{1}$$

where $\mu_0$ is the permeability of free space. We assume that the magnetic field measured by Juno can be described by this simple model. At very low latitudes, the magnetic field direction points approximately in the $z$ direction, with

$$\overrightarrow{B}_{\text{dipole}} = -\frac{\mu_0 m_0}{4\pi}\frac{1}{r^3}\overrightarrow{e_z} = \frac{a}{r^3}\overrightarrow{e_z} \tag{2}$$

Using the empirical model of the equatorial current sheet developed by Pensionerov et al. (2019), when $50\ R_J < \rho \leq 95\ R_J$,

$$I(\rho) = \frac{R_1 I_0}{R_2 \rho} \tag{3}$$

where $R_1$ is 27 $R_J$, $R_2$ is 50 $R_J$, and $I_0 = 26 \times 10^6$ A/$R_J$ is a constant. Equation 3 considers cylindrical magnetic equatorial coordinates, where the $z$-axis coincides with the dipole axis of the internal planetary field and $\rho$ is the perpendicular distance from the axis. Consider the point of low latitude very close to the current sheet (lobe region). Using Equations 1 and 3, we have

$$\overrightarrow{B}_{\text{sheet}} = \frac{\mu_0 I(r)}{2}\overrightarrow{e_{x,y}} = \frac{b}{r}\overrightarrow{e_{x,y}} \tag{4}$$

The direction of the magnetic field is parallel to the equatorial plane and points outward in the radial direction of 5 LT. $B_{\text{lobe}}$ is the superposition of the dipole field and the magnetic field generated by the current sheet. Using the Taylor expansion we can obtain

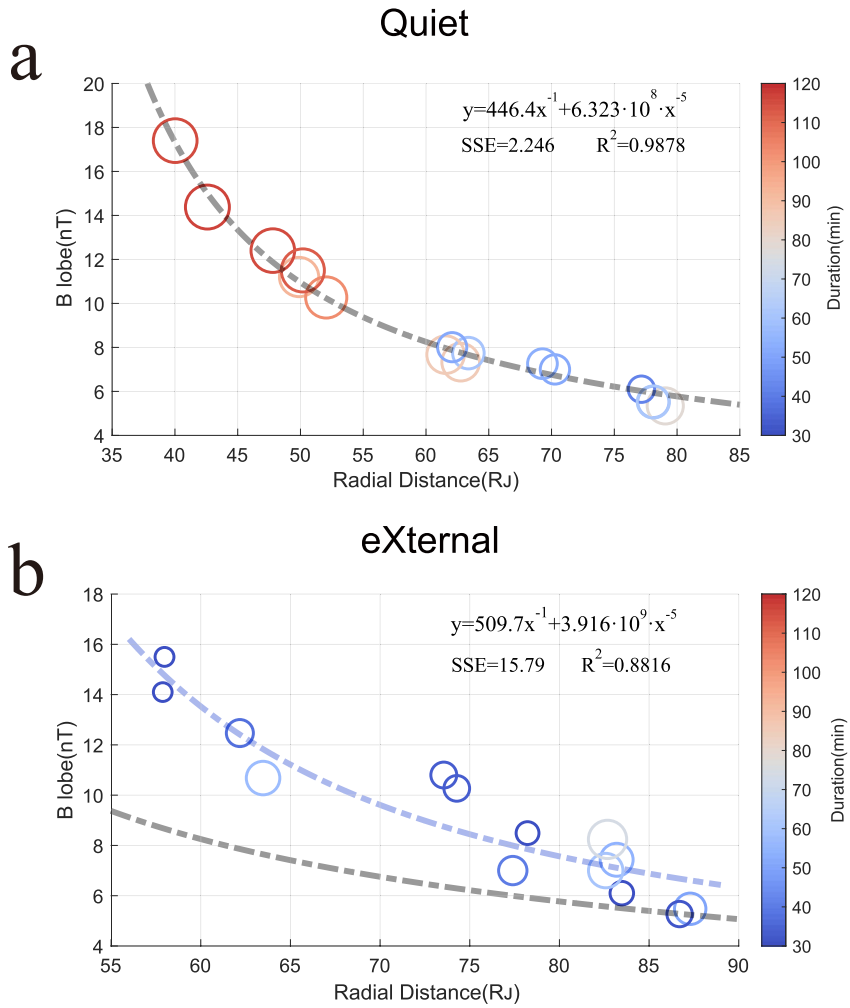


**Figure 2.** Statistical results of Jupiter's current sheet crossing events under different auroral conditions. (a) The magnitude of $B_{\text{lobe}}$ as a function of radial distance before the current sheet crossing for events coincident with auroras under quiet conditions. (b) The magnitude of $B_{\text{lobe}}$ as a function of radial distance before the current sheet crossing for events coincident with auroras under external perturbation conditions. The gray and blue dashed lines represent the curves obtained by fitting the first two terms of Equation 5 under quiet conditions and under external perturbation conditions, respectively, where SSE is the sum of squares for error and $R^2$ is the coefficient of determination.

$$
\begin{aligned}
B_{\text{lobe}} &= \sqrt{\vec{B}_{\text{dipole}}^{\,2} + \vec{B}_{\text{sheet}}^{\,2}} \\
&= \sqrt{\frac{a^2}{r^6} + \frac{b^2}{r^2}} \\
&= \frac{b}{r}\left(1 + \frac{\frac{a^2}{b^2}}{r^4}\right)^{\frac{1}{2}} \\
&= \frac{b}{r} + \frac{\frac{a^2}{2b}}{r^5} + \frac{\frac{a^4}{8b^3}}{r^9}\cdots
\end{aligned}
\tag{5}
$$

Only the first two terms in $1/r$ and $1/r^5$ were kept for simplicity of calculation. Finally, we get the fitted equations for $B_{\text{lobe}}$ and radial distance. As shown in Figures 2a and 2b, the dotted line fits very well with $R^2 = 0.9878$ during quiet conditions. The radial variation in the lobe region magnetic field during quiet periods is applied as

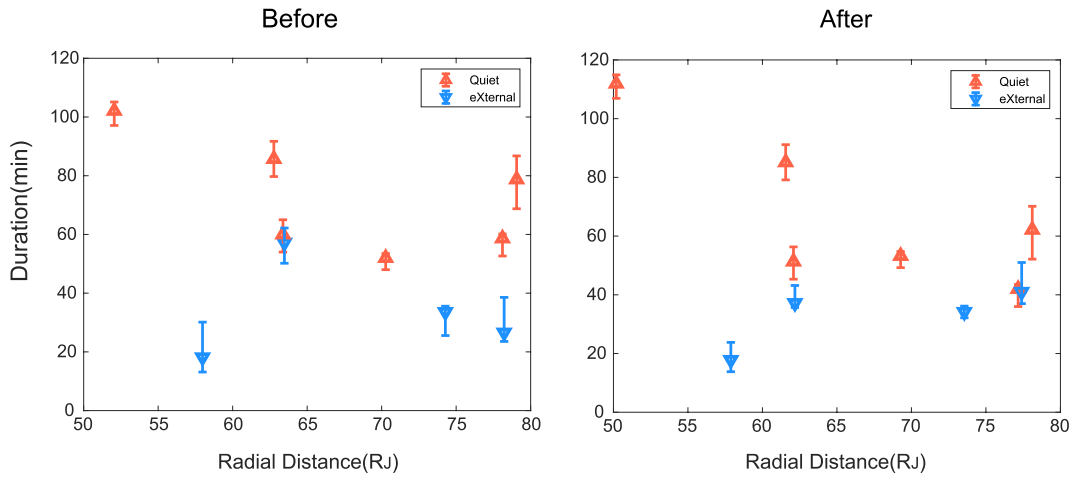


**Figure 3.** The distribution of current sheet crossing durations with error bars in the overlapping radial distance range (50–80 $R_J$) for both quiet (red triangles) and external (blue, upside-down triangles) perturbation conditions before and after auroral observations.

the baseline for Figure 2b. That is, the black dashed lines in Figures 2a and 2b are the same line. The current sheet crossing data corresponding to the aurora during the solar wind compression period is fitted with the blue dashed line in Figure 2b. The blue dashed line shows a good fit with $R^2 = 0.8816$. As indicated in both Connerney et al. (1981, 2020), the $z$ component can be smaller than the dipole value. But this is acceptable because the z-component contribution to $B_{\text{lobe}}$ in the far magnetic tail is very small (the z-component contribution to $B_{\text{lobe}}$ in the simple dipole field is inversely proportional to the fifth power of the radial distance as can be seen from Equation 5). Comparing the blue and black lines two conclusions can be drawn: (a) $B_{\text{lobe}}$ under compressed conditions is clearly larger than that during the quiet period, which shows that the height-integrated current density (hereafter current intensity, measured in $A/R_J$) in the current sheet is enhanced under solar wind compression, as will be discussed in Section 3; (b) the duration of the spacecraft current sheet crossing is roughly longer in the quiet period.

Figure 3 displays the distribution of current sheet crossing durations in the overlapping radial distance range (50–80 $R_J$) for quiet and externally perturbed periods before and after each auroral observation as a function of radial distance. The error bars in Figure 3 represent the uncertainty associated with the identification of each current sheet crossing using both magnetic field information and plasma information. These error bars provide a visual representation of the potential range for the crossing duration. In the overlapping radial distance range for two conditions, the average values of the current sheet crossing duration before and after the aurora under quiet conditions are 72.9 and 67.6 min. Under external perturbation conditions, the average values of duration are 33.9 and 32.5 min, before and after the aurora, respectively. As shown in Figure 3, the duration of the current sheet crossing during the quiet period is clearly larger than during the period of solar wind external perturbations. The result indicates that during solar wind compressional perturbations, the Jupiter current sheet exhibits a distinct thinning. Histograms of crossing duration distributions for all radial distance ranges under both quiet and external disturbance conditions are shown in Figure S2 in Supporting Information S1.

## 3. Discussion and Conclusion

To understand the impact of the solar wind on the Jovian magnetosphere and the role of external drivers in controlling the dynamics of giant, rapidly rotating magnetospheres in general, it is critical to characterize the response of the current sheet. In this study, we have used context from HST observations alongside simultaneous Juno measurements to perform a statistical investigation of Jupiter's dawn-side current sheets properties under solar wind compressions and quiet conditions. The results reveal that Jupiter's dawn-side current sheet thins during the solar wind compression period compared to the quiet period. Figure 4b depicts a cartoon diagram illustrating the corresponding process. For some events under external perturbation conditions, the current sheet can be very dynamic. For example, there are times when Juno crosses the current sheet several times in a short period

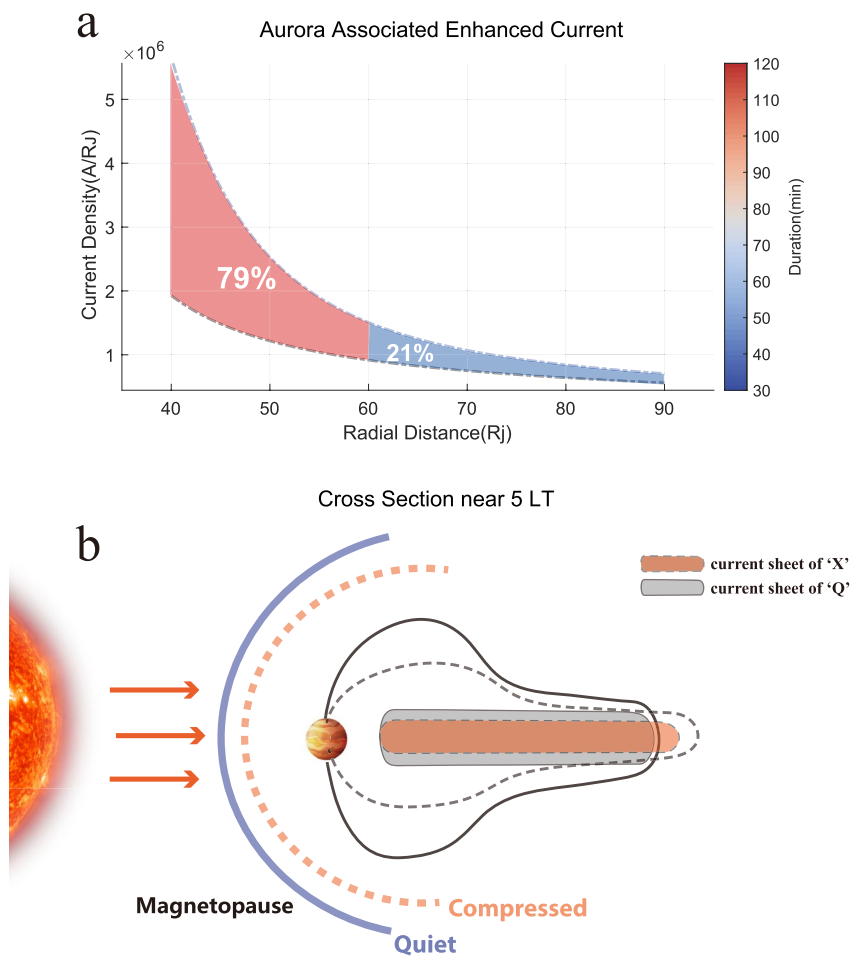


**Figure 4.** (a) Distribution of increased current intensity at different radial distances from aurora under quiet conditions (bottom dashed line) to aurora under solar wind compression (top dashed line); (b) Cartoon schematic of the current sheet under solar wind compression becoming thinner than the current sheet under the quiet period near 5 LT.

and is not steadily entering the lobe region (shown in Figures S11, S15, and S17 in Supporting Information S1). This phenomenon can be caused by the flapping of the thin current sheet, as reported in previous studies (e.g., Volwerk et al., 2013). To address this issue, we set an upper limit on the crossing duration by determining where the spacecraft first enters and last exits the current sheet. Therefore, the actual thickness of the current sheet under an strong external perturbation is only likely to be thinner than what we sampled, and our measurements are likely to provide upper limits to the thickness, so that the relationship may be stronger than that we report. Still, we should be careful about the unexpected effects of current sheet flapping that may occur under external perturbation conditions.

Furthermore, the result shows that $B_{\mathrm{lobe}}$ significantly increases under compressed conditions, indicating that the total current intensity is enhanced during compression-related external perturbations. The increase in current from the quiet magnetosphere to the compressed magnetosphere can be estimated from the distribution of magnetic strength in the lobe region. Figure 4a shows a schematic diagram of the enhanced currents within Jupiter's current sheet from the quiet periods to the solar wind compression periods. $B_{\mathrm{lobe}}$ in Figure 2 is used to infer the current intensities (according to Equation 1) shown in Figure 4a. Again, the gray and blue lines refer to the best-fit radial variation in the current intensity under quiet and externally perturbed conditions, respectively. The red and blue sections between the best-fit current intensity profiles show how much the current intensity increases during the solar wind compression relative to the quiet conditions, that is, the current added to the current sheet during the solar wind compression. The current enhancement from 40 to 90 $R_J$ is calculated to be $4 \times 10^6$ A, of which the current enhancement from 40 to 60 $R_J$ is $3.15 \times 10^6$ A, accounting for 79% of the total enhancement

current, and the enhancement current from 60 to 90 $R_J$ is $8.51 \times 10^5$ A, accounting for 21% of the total enhancement current. The results exhibit that the vast majority of the total current increase during solar wind compression is concentrated in the magnetosphere in the range of 40–60 $R_J$. According to Joy et al. (2002), the most probable magnetopause standoff distance is 63 $R_J$ at 12 LT, therefore the region 40–60 $R_J$ is expected to be well within the magnetopause at 5 LT. In contrast, the total current intensity for quiet conditions from 40 to 90 $R_J$ is $4.7 \times 10^6$ A. In this study, there is an implicit hypothesis that the variations of the perpendicular current (the total currents include the radial current and the azimuthal current) potentially correspond to the variations of the FAC, which is directly related to auroral enhancement. And our findings do suggest a high correlation between the perpendicular currents and auroral enhancement in Jupiter's dawnside current sheet (in agreement with results of Nichols & Cowley, 2022), and suggest a close relationship between the perpendicular currents and FACs. Further research is needed to investigate the current loop associated with aurora enhancement.

In conclusion, the main results are summarized as follows:

1. In this study, we investigated the nature of Jupiter's dawnside current sheet using in-situ magnetic field data during times of known Jovian auroral morphologies as determined by HST observations (Grodent et al., 2018). The measured radial profiles in the magnetic field during "Quiet" or "eXternal" types of the aurora are nicely fitted by an empirical current sheet model, suggesting that magnetospheric conditions were highly consistent for their respective auroral conditions (either "Quiet" or "eXternal").
2. We found that the lobe magnetic field was consistently higher during "eXternal" auroral events, corresponding to enhanced magnetospheric currents than during Quiet auroral events.
3. We estimate the changing magnetospheric currents between "eXternal" and "Quiet" auroral morphologies. We find that the enhancement in current intensity from 40 to 90 $R_J$ is $\sim 4 \times 10^6$ A. And in the region between 40 and 60 $R_J$ which is well inside the magnetopause, the enhanced current accounts for 79% of the total enhanced current.

## Data Availability Statement

The Juno data presented in this study are available from NASA's Planetary Data System as part of the JNO-J-3-FGM-CAL-V1.0 (https://pds-ppi.igpp.ucla.edu/search/view/?f=yes&id=pds://PPI/JNO-J-3-FGM-CAL-V1.0), and JNO-J-JED-3-CDR-V1.0 (https://pds-ppi.igpp.ucla.edu/search/view/?f=yes&id=pds://PPI/JNO-J-JED-3-CDR-V1.0) data sets for the MAG, and JEDI instruments. The model outputs used to generate the figures for analysis presented in this paper are publicly available online (https://doi.org/10.17605/OSF.IO/BDZYF).

**Acknowledgments**
Z. Y. acknowledges the National Science Foundation of China (Grant 42074211) and Key Research Program of the Institute of Geology & Geophysics CAS (Grant IGGCAS-201904). SVB was supported by STFC Grant ST/V000748/1 and ST/M005534/1. WRD is supported by STFC Ernest Rutherford Fellowship ST/W003449/1. B. B. is a Research Associate of the Fonds de la Recherche Scientifique—FNRS. Y. X. very much appreciates the fruitful discussion with Dr. J. E. P. Connerney.

## References

Badman, S. V., Bonfond, B., Fujimoto, M., Gray, R. L., Kasaba, Y., Kasahara, S., et al. (2016). Weakening of Jupiter's main auroral emission during January 2014. *Geophysical Research Letters*, *43*(3), 988–997. https://doi.org/10.1002/2015gl067366

Ballester, G. E., Clarke, J. T., Trauger, J. T., Harris, W. M., Stapelfeldt, K. R., Crisp, D., et al. (1996). Time-resolved observations of Jupiter's far-ultraviolet aurora. *Science*, *274*(5286), 409–413. https://doi.org/10.1126/science.274.5286.409

Baron, R. L., Owen, T., Connerney, J. E. P., Satoh, T., & Harrington, J. (1996). Solar wind control of Jupiter's H+ 3auroras. *Icarus*, *120*(2), 437–442. https://doi.org/10.1006/icar.1996.0063

Bonfond, B., Yao, Z., & Grodent, D. (2020). Six pieces of evidence against the corotation enforcement theory to explain the main aurora at Jupiter. *Journal of Geophysical Research: Space Physics*, *125*(11), e2020JA028152. https://doi.org/10.1029/2020ja028152

Connerney, J. E. P., Benn, M., Bjarno, J., Denver, T., Espley, J., Jorgensen, J., et al. (2017). The Juno magnetic field investigation. *Space Science Reviews*, *213*(1–4), 39–138. https://doi.org/10.1007/s11214-017-0334-z

Connerney, J. E. P., Satoh, T., & Baron, R. L. (1996). Interpretation of auroral "lightcurves" with application to Jovian H+ 3emissions. *Icarus*, *122*(1), 24–35. https://doi.org/10.1006/icar.1996.0107

Connerney, J. E. P., Acuna, M. H., & Ness, N. F. (1981). Modeling the Jovian current sheet and inner magnetosphere. *Journal of Geophysical Research*, *86*(A10), 8370–8384. https://doi.org/10.1029/ja086ia10p08370

Connerney, J. E. P., Timmins, S., Herceg, M., & Joergensen, J. L. (2020). A Jovian magnetodisc model for the Juno era. *Journal of Geophysical Research: Space Physics*, *125*(10), e2020JA028138. https://doi.org/10.1029/2020ja028138

Cowley, S. W. H., & Bunce, E. J. (2001). Origin of the main auroral oval in Jupiter's coupled magnetosphere-ionosphere system. *Planetary and Space Science*, *49*(10–11), 1067–1088. https://doi.org/10.1016/s0032-0633(00)00167-7

Cowley, S. W. H., Nichols, J. D., & Andrews, D. J. (2007). Modulation of Jupiter's plasma flow, polar currents, and auroral precipitation by solar wind-induced compressions and expansions of the magnetosphere: A simple theoretical model. *Annales Geophysicae*, *25*(6), 1433–1463. https://doi.org/10.5194/angeo-25-1433-2007

Cowley, S. W. H., Provan, G., Bunce, E. J., & Nichols, J. D. (2017). Magnetosphere-ionosphere coupling at Jupiter: Expectations for Juno Perijove 1 from a steady state axisymmetric physical model. *Geophysical Research Letters*, *44*(10), 4497–4505. https://doi.org/10.1002/2017GL073129

Dunn, W. R., Gray, R., Wibisono, A. D., Lamy, L., Louis, C., Badman, S. V., et al. (2020). Comparisons between Jupiter's X-ray, UV and radio emissions and in-situ solar wind measurements during 2007. *Journal of Geophysical Research: Space Physics*, *125*(6), e2019JA027222. https://doi.org/10.1029/2019ja027222

Gerard, J. C., Grodent, D., Dols, V., Prange, R., Waite, J. H., Gladstone, G. R., et al. (1994). A remarkable auroral event on Jupiter observed in the ultraviolet with the Hubble Space Telescope. *Science*, *266*(5191), 1675–1678. https://doi.org/10.1126/science.266.5191.1675

Grodent, D., Bonfond, B., Yao, Z., Gérard, J.-C., Radioti, A., Dumont, M., et al. (2018). Jupiter's aurora observed with HST during Juno orbits 3 to 7. *Journal of Geophysical Research: Space Physics*, *123*(5), 3299–3319. https://doi.org/10.1002/2017JA025046

Gurnett, D. A., Kurth, W. S., Hospodarsky, G. B., Persoon, A. M., Zarka, P., Lecacheux, A., et al. (2002). Control of Jupiter's radio emission and aurorae by the solar wind. *Nature*, *415*(6875), 985–987. https://doi.org/10.1038/415985a

Hill, T. W. (1979). Inertial limit on corotation. *Journal of Geophysical Research*, *84*(A11), 6554–6558. https://doi.org/10.1029/ja084ia11p06554

Joy, S. P., Kivelson, M. G., Walker, R. J., Khurana, K. K., Russell, C. T., & Ogino, T. (2002). Probabilistic models of the Jovian magnetopause and bow shock locations. *Journal of Geophysical Research*, *107*(A10), SMP-17.

Khurana, K. K., & Schwarzl, H. K. (2005). Global structure of Jupiter's magnetospheric current sheet. *Journal of Geophysical Research*, *110*(A7), A07227. https://doi.org/10.1029/2004ja010757

Kimura, T., Badman, S., Tao, C., Yoshioka, K., Murakami, G., Yamazaki, A., et al. (2015). Transient internally driven aurora at Jupiter discovered by Hisaki and the Hubble Space Telescope. *Geophysical Research Letters*, *42*(6), 1662–1668. https://doi.org/10.1002/2015GL063272

Kimura, T., Nichols, J. D., Gray, R., Tao, C., Murakami, G., Yamazaki, A., et al. (2017). Transient brightening of Jupiter's aurora observed by the Hisaki satellite and Hubble Space Telescope during approach phase of the Juno spacecraft. *Geophysical Research Letters*, *44*(10), 4523–4531. https://doi.org/10.1002/2017GL072912

Kita, H., Kimura, T., Tao, C., Tsuchiya, F., Misawa, H., Sakanoi, T., et al. (2016). Characteristics of solar wind control on Jovian UV auroral activity deciphered by long-term Hisaki EXCEED observations: Evidence of preconditioning of the magnetosphere? *Geophysical Research Letters*, *43*(13), 6790–6798. https://doi.org/10.1002/2016GL069481

Krupp, N., Lagg, A., Woch, J., Krimigis, S. M., Livi, S., Mitchell, D. G., & Dougherty, M. K. (2005). The Saturnian plasma sheet as revealed by energetic particle measurements. *Geophysical Research Letters*, *32*(20), L20S03. https://doi.org/10.1029/2005gl022829

Krupp, N., Vasyliunas, V. M., Woch, J., Lagg, A., Khurana, K. K., Kivelson, M. G., et al. (2004). Dynamics of the Jovian magnetosphere. *Jupiter: The Planet, Satellites and Magnetosphere*, *1*, 617–638.

Liu, Z. Y., Zong, Q. G., Blanc, M., Sun, Y. X., Zhao, J. T., Hao, Y. X., & Mauk, B. H. (2021). Statistics on Jupiter's current sheet with Juno data: Geometry, magnetic fields and energetic particles. *Journal of Geophysical Research: Space Physics*, *126*(11), e2021JA029710. https://doi.org/10.1029/2021ja029710

Mauk, B. H., Haggerty, D. K., Jaskulek, S. E., Schlemm, C. E., Brown, L. E., Cooper, S. A., et al. (2017). The Jupiter energetic particle detector instrument (JEDI) investigation for the Juno mission. *Space Science Reviews*, *213*(1), 289–346. https://doi.org/10.1007/s11214-013-0025-3

Mauk, B. H., Mitchell, D. G., McEntire, R. W., Paranicas, C. P., Roelof, E. C., Williams, D. J., & Lagg, A. (2004). Energetic ion characteristics and neutral gas interactions in Jupiter's magnetosphere. *Journal of Geophysical Research*, *109*(A9), A09S12. https://doi.org/10.1029/2003ja010270

Nichols, J. D., Clarke, J. T., Gérard, J. C., Grodent, D., & Hansen, K. C. (2009). Variation of different components of Jupiter's auroral emission. *Journal of Geophysical Research*, *114*, A06210. https://doi.org/10.1029/2009ja014051

Nichols, J. D., & Cowley, S. W. H. (2003). Magnetosphere-ionosphere coupling currents in Jupiter's middle magnetosphere: Dependence on the effective ionospheric Pedersen conductivity and iogenic plasma mass outflow rate. *Annales Geophysicae*, *21*(7), 1419–1441. https://doi.org/10.5194/angeo-21-1419-2003

Nichols, J. D., & Cowley, S. W. H. (2022). Relation of Jupiter's dawnside main emission intensity to magnetospheric currents during the Juno mission. *Journal of Geophysical Research: Space Physics*, *127*(1), e2021JA030040. https://doi.org/10.1029/2021JA030040

Nichols, J. D., Yeoman, T. K., Bunce, E. J., Chowdhury, M. N., Cowley, S. W. H., & Robinson, T. R. (2017). Periodic emission within Jupiter's main auroral oval. *Geophysical Research Letters*, *44*(18), 9192–9198. https://doi.org/10.1002/2017GL074824

Pan, D. X., Yao, Z. H., Manners, H., Dunn, W., Bonfond, B., Grodent, D., et al. (2021). Ultralow-frequency waves in driving Jovian aurorae revealed by observations from HST and Juno. *Geophysical Research Letters*, *48*(5), e2020GL091579. https://doi.org/10.1029/2020gl091579

Pensionerov, I. A., Alexeev, I. I., Belenkaya, E. S., Connerney, J. E. P., & Cowley, S. W. H. (2019). Model of Jupiter's current sheet with a piecewise current density. *Journal of Geophysical Research: Space Physics*, *124*(3), 1843–1854. https://doi.org/10.1029/2018ja026321

Pensionerov, I. A., Belenkaya, E. S., & Alexeev, I. I. (2021). A model of Jupiter's current disk optimized for Juno and Galileo magnetic field data. *Cosmic Research*, *59*(3), 175–182. https://doi.org/10.1134/s0010952521030084

Pensionerov, I. A., Cowley, S. W., Belenkaya, E. S., & Alexeev, I. I. (2021). Axially Asymmetric steady state model of Jupiter's magnetosphere-ionosphere coupling. *Journal of Geophysical Research: Space Physics*, *126*(11), e2021JA029608. https://doi.org/10.1029/2021ja029608

Pryor, W. R., Stewart, A. I. F., Esposito, L. W., McClintock, W. E., Colwell, J. E., Jouchoux, A. J., et al. (2005). Cassini UVIS observations of Jupiter's auroral variability. *Icarus*, *178*(2), 312–326. https://doi.org/10.1016/j.icarus.2005.05.021

Ray, L. C., Achilleos, N. A., Vogt, M. F., & Yates, J. N. (2014). Local time variations in Jupiter's magnetosphere-ionosphere coupling system. *Journal of Geophysical Research: Space Physics*, *119*(6), 4740–4751. https://doi.org/10.1002/2014JA019941

Ray, L. C., Ergun, R. E., Delamere, P. A., & Bagenal, F. (2010). Magnetosphere-ionosphere coupling at Jupiter: Effect of field-aligned potentials on angular momentum transport. *Journal of Geophysical Research*, *115*(A9), A09211. https://doi.org/10.1029/2010JA015423

Saur, J., Janser, S., Schreiner, A., Clark, G., Mauk, B. H., Kollmann, P., et al. (2018). Wave-particle interaction of Alfvén waves in Jupiter's magnetosphere: Auroral and magnetospheric particle acceleration. *Journal of Geophysical Research: Space Physics*, *123*(11), 9560–9573. https://doi.org/10.1029/2018ja025948

Sinclair, J., Orton, G., Fernandes, J., Kasaba, Y., Sato, T., Fujiyoshi, T., et al. (2019). A brightening of Jupiter's auroral 7.8-μm CH 4 emission during a solar-wind compression. *Nature Astronomy*, *1*(7), 607–613. https://doi.org/10.1038/s41550-019-0743-x

Southwood, D. J., & Kivelson, M. G. (2001). A new perspective concerning the influence of the solar wind on the Jovian magnetosphere. *Journal of Geophysical Research*, *106*(A4), 6123–6130. https://doi.org/10.1029/2000ja000236

Thomas, N., Bagenal, F., Hill, T. W., & Wilson, J. K. (2004). The Io neutral clouds and plasma torus. *Jupiter. The Planet, Satellites and Magnetosphere*, *1*, 561–591.

Volwerk, M., Andre, N., Arridge, C. S., Jackman, C. M., Jia, X., Milan, S. E., et al. (2013). Comparative magnetotail flapping: An overview of selected events at Earth, Jupiter and Saturn. *Annales Geophysicae*, *31*(5), 817–833. https://doi.org/10.5194/angeo-31-817-2013

Yao, Z. H., Bonfond, B., Clark, G., Grodent, D., Dunn, W., Vogt, M., et al. (2020). Reconnection and dipolarization driven auroral dawn storms and injections. *Journal of Geophysical Research: Space Physics*, *125*(8), e2019JA027663. https://doi.org/10.1029/2019JA027663

Yao, Z. H., Bonfond, B., Grodent, D., Chané, E., Dunn, W. R., Kurth, W. S., et al. (2022). On the relation between auroral morphologies and compression conditions of Jupiter's magnetopause: Observations from Juno and the Hubble Space Telescope. *Journal of Geophysical Research: Space Physics*, *127*(10), e2021JA029894. https://doi.org/10.1029/2021JA029894

Yao, Z. H., Grodent, D., Kurth, W. S., Clark, G., Mauk, B. H., Kimura, T., et al. (2019). On the relation between Jovian aurorae and the loading/unloading of the magnetic flux: Simultaneous measurements from Juno, Hubble Space Telescope, and Hisaki. *Geophysical Research Letters*, *46*(21), 11632–11641. https://doi.org/10.1029/2019GL084201